Available online at www.sciencedirect.com

ScienceDirect

journal homepage: www.elsevier.com/locate/he

Hydrogen turbulent nonpremixed flames blended with spray or prevapourised biofuels

Yilong Yin [a,*], Paul R. Medwell [a], Bassam B. Dally [b]

[a] School of Mechanical Engineering, The University of Adelaide, Adelaide, South Australia 5005, Australia
[b] Clean Combustion Research Centre, King Abdullah University of Science and Technology, Thuwal 23955-6900, Kingdom of Saudi Arabia

HIGHLIGHTS

- Spray flame exhibits higher global luminosity and radiant fraction than vapour flame.
- NO_x emissions increase with biofuel addition via thermal and prompt NO formation.
- Cyclic monoterpene biofuels have higher NO_x emissions than aromatic biofuels.
- Reducing H_2 concentration leads to large increase in luminosity and radiant fraction.

GRAPHICAL ABSTRACT

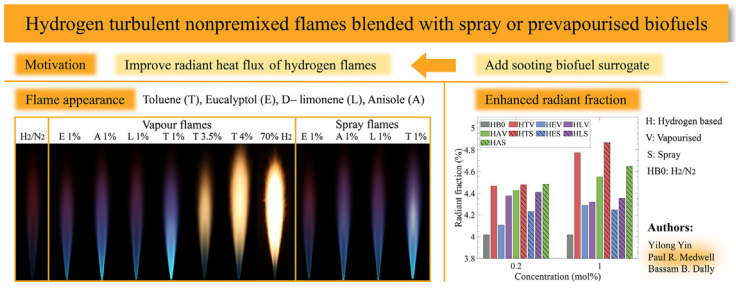

ARTICLE INFO

Article history:
Received 24 November 2022
Received in revised form
12 March 2023
Accepted 15 March 2023
Available online 6 April 2023

Keywords:
Hydrogen
Biofuel
Spray flame
Radiant heat flux
NO_x emissions

ABSTRACT

The low radiant intensity of hydrogen flames may be enhanced by adding biofuels with a high sooting propensity. This paper reports the effect of biofuel concentration and phase on the combustion characteristics of turbulent nonpremixed hydrogen-based flames. The 0.2 and 1 mol% vapourised/spray biofuel surrogates blended flames exhibit limited soot loading, except for 1 mol% spray toluene and anisole blends where soot starts to form. Spray additives benefit the formation of soot by creating localised fuel-rich conditions. Blending 3.5 and 4 mol% vapourised toluene attains a sooting flame and significantly enhances the luminosity and radiant fraction. The global NO_x emissions increase with prevapourised/spray biofuel surrogates due to the enhanced NO formation via thermal and prompt routes. Reducing the hydrogen concentration from 9:1 to 7:3 in H_2/N_2 (by mole) leads to large increases in luminosity and radiant fraction by 34 times and 135%, respectively, and a reduction in NO_x emissions by 68%.

* *Corresponding author*:
E-mail address: yilong.yin@adelaide.edu.au (Y. Yin).

https://doi.org/10.1016/j.ijhydene.2023.03.232

Nomenclature

χ_r	Radiant fraction
$\dot{m}$	Mass flow rate, kg/s
$\dot{Q}_F$	Total thermal power, kW
$\dot{Q}_r$	Radiated heat, kW
$\dot{q}''$	Radiant heat flux, kW/m^2
ρ	Density, kg/m^3
σ	Surface tension, N/m
c	Empirical constant dependent on the nebuliser type
d	Inner diameter of the jet, m
EI	Emission index
F	Ultrasound frequency of the nebuliser, Hz
L_f	Flame length, mm
MW	Molecular weight, g/mol
n_c	Carbon concentration of fuel
T	Temperature, K
U/d	Exit strain rate, s^{-1}
U	Mean velocity, m/s
CEM	Controlling evaporating mixing
CO	Carbon monoxide
CO_2	Carbon dioxide
CO_{2amb}	Mole fraction of CO_2 in ambient air
DAQ	Data acquisition systems
H_2	Hydrogen
H_2O	Water
HAB	Height above burner, mm
LHV	Lower heating value, MJ/kg
N_2	Nitrogen
NO	Nitric oxide
NO_2	Nitrogen dioxide
OPPDIF	Opposed-flow diffusion flame
PAHs	Polycyclic aromatic hydrocarbons
ROP	Rate of production
SMD	Sauter mean diameter

Introduction

As the world is shifting away from carbon-emitting processes, using hydrogen as a renewable energy carrier to replace conventional fuels, both in domestic and industrial sectors, is emerging as a promising approach [1–4]. Hydrogen has been widely studied as a diluent to reduce soot production in combustion systems such as gas turbines and internal combustion engines, by taking advantage of its carbon-free nature [5–10]. The effects of hydrogen addition on soot production can be attributed to three mechanisms: thermal effect, dilution effect, and chemical effect [11–13]. It has been reported that adding hydrogen to hydrocarbon flames increases the global flame temperature, and hence reduces soot by promoting soot oxidation via thermal effect [14,15]. The dilution effect of hydrogen addition reduces soot production by decreasing the carbon concentration per unit volume of the fuel mixture [11,16]. Previous studies have indicated that a portion of hydrogen can be blended into natural gas supply networks as a diluent to mitigate CO_2 emissions [17]. There is an increasing demand for achieving a more complete replacement of fossil fuels in a broader range of applications, as countries and companies are pledging to attain net zero emissions. Therefore, the work in this study is dedicated to identifying the challenges of using hydrogen as a primary energy source in practical applications and evaluating potential solutions.

A major challenge for replacing conventional fuels with hydrogen in high-temperature practical applications is the low thermal radiation from hydrogen flames due to the absence of soot. Thermal radiation is the transfer of heat energy through electromagnetic radiation and is a significant mode of heat transfer in many practical combustion systems (e.g., furnaces and boilers). The low radiant heat flux of hydrogen flames makes it difficult to effectively transfer heat from the flame to surrounding materials, reducing the efficiency of these systems [18–21]. One possible approach to compensate for this disadvantage of hydrogen flames in practical applications is to blend hydrogen with highly sooting additives to promote soot formation in the flame. Hence, the radiant intensity of the flame can be enhanced via efficient blackbody radiation from soot particulates [19,22,23].

Biofuels with high sooting propensities can be chosen as suitable additives since they are generally comprised of abundant aromatics, which favour the formation of soot precursors — polycyclic aromatic hydrocarbons (PAHs). In addition, the raw materials for their production can be harvested from the by-products and waste products from the existing industries, such as pulp industries and food production plants [24,25]. Bio-oils and essential oils are the two types of biofuels focused in this paper for their abundant aromatics, sooting propensity, and accessibility. Bio-oils are obtained from fast pyrolysis of lignin and cellulose multicomponent mixtures chemically comprised of substantial amounts of phenolic compounds, toluene, anisole and furan [26]. Lignin in their feedstock is the source for the synthesis of phenolic chemicals [27]. Essential oils are mainly comprised of terpenes $(C_5H_8)_n$, including monoterpenes (C10), sesquiterpenes (C15) and diterpenes (C20), which are biosynthesised via five-carbon isoprene units [28].

Efforts have been dedicated to evaluating the efficacy of adding sooting hydrocarbons to hydrogen-based flames on radiative heat transfer enhancement. Adding pulverised bituminous coal could improve the radiative properties of a hydrogen-coal flame because the heavy hydrocarbons (tar) produced from coal pyrolysis promote soot formation [22]. Highly radiating hydrogen-based flames were previously achieved by adding 1–5 mol% toluene [19]. Adding toluene as a soot-generating additive has significantly increased soot volume fraction in a hydrogen-nitrogen (1:1 vol) jet flame with a bulk mean Reynolds number of 5000. Gee et al. [23] further investigated the effect of toluene addition to pure hydrogen flames at 10,000 Reynolds number on a bluff-body burner. By comparing the thermal radiation of natural gas flame established on the same burner, approximately 4% vapourised toluene is required for H_2 flames to attain an equivalent radiant heat flux of a natural gas flame. These studies provided a preliminary assessment of the efficacy of this approach. However, the additives tested in these studies are

limited by heavy hydrocarbons and toluene. As discussed in the previous paragraph, biofuels, including bio-oils and essential oils, can be used as suitable additives to enhance the radiant heat flux of hydrogen flames. Yin et al. [29] investigated the sooting propensity of biofuel surrogates (eucalyptol, limonene, and anisole) on a wick-fed burner and demonstrated their potential to be used as soot-enhancing additives for hydrogen-based flames through combined experimental and numerical methods. The findings indicated that, although these biofuel surrogates have less sooting propensity than toluene, they enhance the radiant fraction of the H_2/N_2 flame by 2–19%. However, there is still a lack of quantitative measurements of the radiant heat flux enhancement. In addition, the influencing factors of the radiation enhancement, such as the chemical structure of additives, concentration, Reynolds number and exit strain rate are largely unavailable.

In addition to the issues around low radiation from the absence of soot, another challenge associated with hydrogen adaptation into practical applications is the increased NO_x emissions. The higher flame temperature of hydrogen promotes the formation of thermal NO_x by providing the required high activation energy of the NO route: $O + N_2 \rightleftharpoons NO + N$, which initiates the NO formation [30]. However, fuel and prompt NO_x are avoided when using hydrogen as the fuel [31,32]. Although hydrogen flames are often associated with higher NO_x emissions, the impact of biofuel blending (e.g., through the lower flame temperature due to increased heat radiation) is not well understood. None of the studies reported the efficacy of blending additives to hydrogen flames on radiant intensity enhancement along with the potential challenge of NO_x emissions.

To introduce additives to hydrogen flames in practical applications, liquid fuels could be sprayed directly into the flame or entrained by the gaseous fuel. Whether the additives are introduced in the gaseous or liquid phase — by prevapourisation or atomisation, respectively — may have a significant impact on soot production, NO_x and CO emissions [19,33]. Reduced soot production and NO_x emissions were observed in nonpremixed flames established on a burner that promotes prevapourisation of palm methyl ester fuel droplets [33]. Under turbulent nonpremixed conditions, the local fuel-rich mixture generated by fuel droplets from atomisation promotes the formation of aromatics and ultimately soot [34]. A more detailed comparison between spray and prevapourisation for introducing toluene into turbulent nonpremixed hydrogen flames was conducted to study their influence on soot evolution [19]. Substantially more polycyclic aromatic hydrocarbons and soot are formed near the nozzle exit plane in spray flames than prevapourised flames [19]. Investigation of these two methods using liquid biofuels with different properties can provide valuable knowledge for future applications.

Since biofuels are usually comprised of complex compositions and various properties ascribed to the different feedstocks and production methods, directly using biofuels inevitably introduces challenges for fundamental-level studies of the chemical effects [24]. Therefore, surrogates that can emulate the various properties of complex fuels are widely employed in experimental and numerical research [35,36]. Four different surrogates (see chemical structures in Fig. 1) are chosen in this study to emulate the combustion properties of bio-oils and essential oils. Toluene (C_7H_8), together with other aromatics, are the main components in bio-oils [19]. Anisole (C_7H_8O) is the characteristic of lignin structures and is recognised as the main source in forming aromatics during the production of bio-oils [37]. In addition, anisole is usually used to emulate the evolution of methoxy phenol, a key precursor of PAH and soot in biomass combustion [37]. Cyclic monoterpenes — eucalyptol ($C_{10}H_{18}O$) and D-limonene ($C_{10}H_{16}$) — are the primary components in eucalyptus oil and orange oil, accounting for 90 wt% and 97 wt%, respectively [38].

The efficacy of adding sooting hydrocarbons to enhance the low radiant heat flux of hydrogen flames for practical systems has been established. However, previous studies that focussed on this approach either only achieved a Reynolds number of 5000 [19], tested only a limited variety of additives [19,23], or did not consider the potential challenge of NO_x emissions [29]. Furthermore, the influencing factors such as hydrogen concentration, bulk mean exit strain rate, and their correlation to the flame characteristics are not well understood. In this paper, the combustion characteristics, including flame appearance, radiant heat flux, flame temperature, and NO_x emissions of turbulent nonpremixed hydrogen-nitrogen flames, blended with four different prevapourised or sprayed biofuel surrogates, are investigated. Qualitative and quantitative evaluation of introduction methods, biofuel surrogates' concentrations, and hydrogen concentrations deepen the understanding of dominating factors in achieving radiating hydrogen flames, along with the aforementioned flame characteristics. In particular, the experimental and numerical investigations of NO_x formation in these blended hydrogen flames provide insights into the potential challenge of this approach. Future experimental work using laser-based diagnostic techniques to measure the instantaneous flame temperature, OH^*, distribution of liquid droplets, soot volume fraction, and soot sizing can yield a better understanding of soot evolution in these blended flames.

Methodology

Burner configuration

An integrated vapourised/spray jet flame burner, shown in Fig. 2a, supplied biofuels as either droplets or vapour. An ultrasonic nebuliser was installed in a holder with an exterior smooth contraction, which was in turn inserted in a housing with an internal smooth contraction. A 5.5-mm-internal-diameter jet was located at the top of the housing and axially aligned with the nebuliser exit. In the prevapourisation configuration, liquid biofuel surrogate was prevapourised by a controlling evaporating mixing (CEM) unit heated to 190 °C upstream of the burner and mixed with a 9:1 mixture of H_2/N_2 gases. The liquid fuel inlet was blocked in this configuration.

In the spray flame configuration, the H_2/N_2 mixture was supplied as a carrier gas through the gas inlet of the burner and transported the biofuel-surrogate droplets generated by the ultrasonic nebuliser with minimal initial momentum to the flame. The gas and liquid flow rates were controlled by

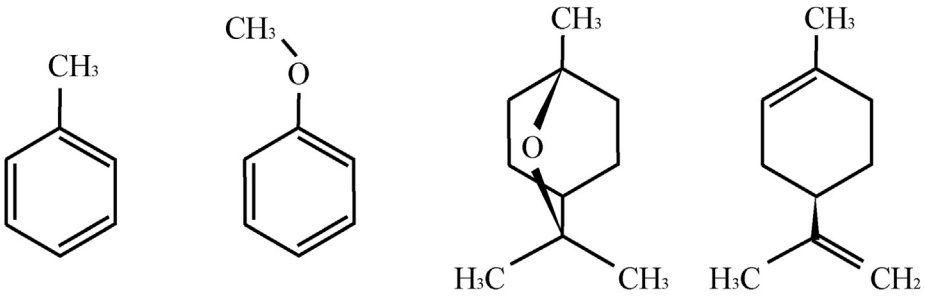

(a) Toluene (b) Anisole (c) Eucalyptol (d) D-limonene

Fig. 1 – Chemical structure of biofuel surrogates.

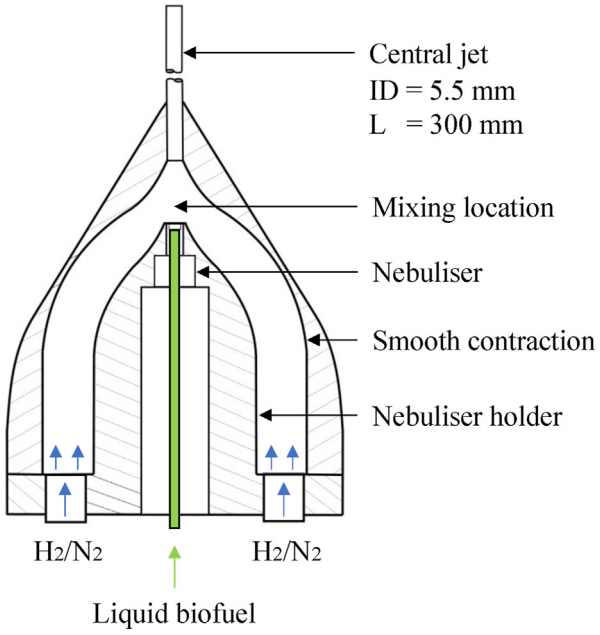

(a) Integrated vapourised/spray burner.

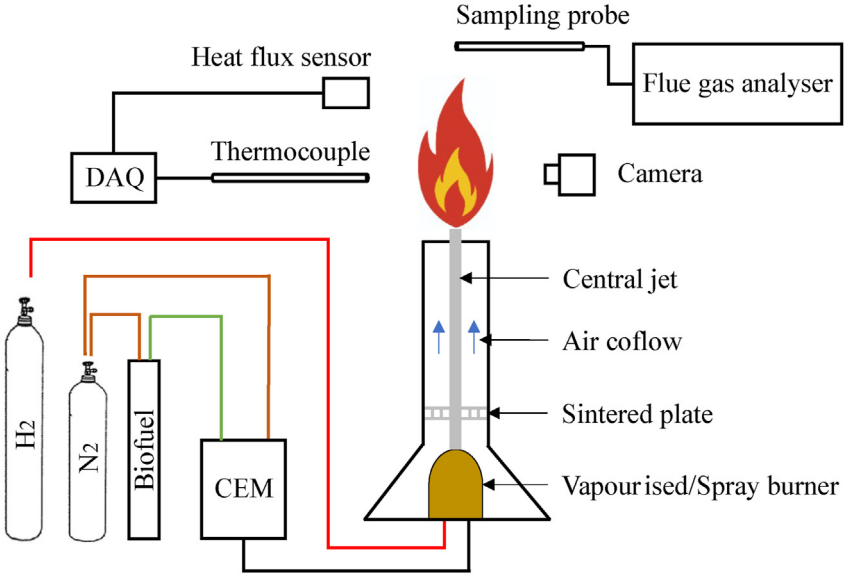

(b) Schematic of the experimental setup.

Fig. 2 – Schematic of the vapourised/spray burner (2a) and the experimental setup (2b).

mass flow controllers (Alicat) with the manufacturer-specified uncertainty of ±0.5% of reading and ±0.2% of full scale. The Sauter mean diameter (SMD) of the biofuel droplets is estimated to be 30 μm at the ultrasonic nebuliser exit based on the data provided by the manufacturer (Sonotek). The SMD of the droplets is calculated from the commonly used equation for ultrasound-induced atomisation [39]:

$$d_{SMD} = c\left(\frac{8\pi\sigma}{\rho F^2}\right)^{\frac{1}{3}} \quad (1)$$

where c is an empirical constant dependent on the nebuliser type, σ is the surface tension, ρ is the density of the liquid, and F is the ultrasound frequency of the nebuliser.

The burner was pre-heated in both vapourised and spray configurations before lighting the flame. A nitrogen carrier gas was heated to 190 °C by the CEM and supplied to the jet. The temperature at the jet exit was measured and maintained at 110±6 °C. At the biofuel surrogate concentrations tested in this work, the partial pressure of the prevapourised biofuel surrogates is lower than their vapour pressure at such temperatures.

Experimental setup

Turbulent nonpremixed flames were stabilised on the vapourised/spray burner. A uniform coflow at 1.0 m/s of room-temperature flowed through a 150 mm × 150 mm square contractor. An exhaust hood was placed at a constant vertical distance (700 mm) above the flame tip. A H_2/N_2 mixture (9:1 by mole) was selected as the non-blended flame case, with a fixed bulk mean Reynolds number of 10,000. Nitrogen was blended with hydrogen to increase the bulk mean Reynolds number of the flames to 10,000. As highly radiating H_2/N_2 (1:1 vol) flames with a Reynolds number of 5000 were achieved previously by blending 1–5% toluene [19], there is a need to investigate the effect of blending biofuels at lower concentrations and compared with higher concentrations. Therefore, the H_2/N_2 mixture was blended with 0.2 and 1% biofuel surrogate (based on the mole concentration of H_2) by prevapourisation and spray. Prevapourised toluene was further tested at 3.5 and 4% as higher concentration cases for comparison. The carbon flow rates between different biofuel/H_2/N_2 mixtures were kept constant for each biofuel surrogate concentration to ensure an equivalent carbon flux. To investigate the effect of lower hydrogen concentration on flame characteristics, a 7:3 H_2/N_2 mixture (by mole) blended by 3.5 mol% vapourised toluene with bulk mean Reynolds number above 10,000 and reduced bulk mean exit velocity was also tested on the same jet. From the 9:1 H_2/N_2 to 7:3 H_2/N_2 mixture, the H_2 flow rate was reduced by half and the N_2 flow rate was increased to maintain a constant bulk mean Reynolds number of 10,000.

Table 2 – Test conditions.

Test parameter	Unit	Result
Ambient temperature	°C	25
Ambient pressure	atm	1
Temperature at the jet exit	°C	110±6
Air coflow	m/s	1
H_2 flow rate	L/min	144
N_2 flow rate	L/min	15
H_2 flow rate (LHTV)	L/min	72
N_2 flow rate (LHTV)	L/min	26

The detailed flame cases are presented along with flame codes in Table 1. The test conditions are shown in Table 2. Due to various chemical and physical properties of biofuel surrogates, the total heat input and Reynolds number of flame cases at the same blending ratio change less than 1%. The non-blended flame is hereafter referred to as "HB0". The blended flame cases, for example, in "HEV/Sx", "HE" indicates that the H_2/N_2 mixture is blended with eucalyptol, "V/S" represents the introduction method — prevapourisation or spray, "x" is the biofuel surrogate concentration used in the case in mol%. In "LHTV", "L" indicates the lower hydrogen concentration. The exit strain rate (U/d) is the ratio between the mean velocity at the jet exit and the inner diameter of the jet [40,41]. The flame length of the non-blended H_2/N_2 flame (HB0) is denoted as L_f in this paper.

Experimental diagnostics

Fig. 2b shows the schematic of the experimental setup. To analyse the effect of biofuel surrogate addition on the appearance of the flames, a digital commercial single-lens reflex camera — Canon 6D with a 50 mm focal length and f/1.8 lens was used. The colour still photographs were converted to grayscale in image post-processing to analyse the luminosity of the flames.

To measure the radiative heat transfer from the flames, two heat flux sensors (Medtherm Corporation model 92241/2) were placed at a radial distance of 284 mm from the centre of the jet. The angular sensitivity of the heat flux sensor was measured prior to the experiment. To minimise the effect of

Table 1 – Flame details and codes of the turbulent nonpremixed non-blended and biofuel surrogate/H_2/N_2 flames. The flame cases and corresponding flames codes are as follows: H_2/N_2/Toluene - HTV/Sx; H_2/N_2/Eucalyptol - HEV/Sx; H_2/N_2/D-limonene - HLV/Sx; H_2/N_2/Anisole - HAV/Sx.

mol%	Heat input	Exit strain rate	Re_{jet}	Flame code
x	(kW)	U/d (s^{-1})	(–)	x = mol%
0.2	24.6	20,300	10,400	HTV/Sx, HEV/Sx, HLV/Sx, HAV/Sx
1.0	28.2	20,500	11,800	HTV/Sx, HEV/Sx, HLV/Sx, HAV/Sx
3.5	37.2	20,900	17,500	HTV
3.5	18.6	12,800	13,200	LHTV
4.0	39.2	21,000	18,600	HTV

angular sensitivity, a 20° view restrictor was used. The uncertainty of the radiant heat flux measurement was reduced to ±3%. The heat flux sensor equipped with a 20° view restrictor measured heat flux from a portion of the flame 100 mm tall at a radial distance of 284 mm. In comparison to measuring the global heat flux of the flame, heat flux data measured at different flame heights can be correlated to the flame temperature data collected at the same flame height to evaluate the potential interferences between these parameters. To compare the effect of different introduction methods — sprayed or prevapourised — on the combustion characteristics between blended flames, the measuring points are designed to focus on the momentum-driven region near the jet exit between height above burner (HAB) 40 mm − 390 mm (i.e., $x/L_f = 0 - 0.4$), with eight equi-spaced measuring points. The heat flux data at each measuring location was recorded for 1 min at 2500 Hz. The error calculated from the data was within ±2%.

To correlate the mean centreline flame temperature to the radiant heat flux and flame appearance, a Type-R thermocouple with a 0.2 mm diameter wire size and a 0.7 mm diameter bare-bead was employed to measure the mean centreline flame temperature between flame cases at the same measuring points as radiant intensity data. The thermocouple flame temperature measurements were corrected for radiation losses. Soot deposition on the thermocouple bead was not observed in the experiment; however, emissivity temperature dependence was considered. The mean centreline flame temperature was recorded after a steady state was achieved. The uncertainty of the mean centreline flame temperature measurement was mainly ascribed to the radiation correction and was estimated to be ±6%. The mean centreline flame temperature at each measuring location was collected for 1 min at 10 Hz after a steady state was achieved. The error calculated from the obtained flame temperature data was ±1%.

A Testo 350 XL flue gas analyser was used to measure and compare the global emissions including CO, CO_2 and NO_x (NO, NO_2) across various flame cases. The resolution of NO, NO_2, CO sensors is 1 ppm, and that of CO_2 measurement is 0.01 vol %. To achieve consistency with sampling across different flame cases, a probe was placed at the centreline of flames with a constant relative distance of 100 mm to collect flue gas samples emitted from the flames. The emission index of NO_x is independent of ambient air dilution because of the normalisation based on carbonaceous species using equation (3). The flue gas analyser was calibrated daily using a gas mixture with a known percentage. In accordance with the manufacturer' specification, the uncertainty of the global emission measurement was within ±2%.

Chemical analysis

To analyse the chemistry (i.e., reaction pathways and chemical mechanisms) contributing to NO_x emissions in the blended H_2/N_2 flames, opposed-flow diffusion (OPPDIF) flames in Chemkin Pro v19.2 was used along with a comprehensive chemical kinetic mechanism for NO_x formation modelling. The chemical kinetic mechanism was developed by CRECK Modelling Group for $C_1 - C_{16}$ hydrocarbon combustion, which comprised 24,501 reactions and 497 species [42]. The results from OPPDIF modelling have been widely coupled with experimental measurements to evaluate the chemistry in jet flames [43,44]. To the best of the authors' knowledge, a chemical kinetics mechanism for comprehensive NO_x formation is not available for all biofuels tested in this work — eucalyptol and D-limonene excluded. Therefore, only toluene and anisole blends were analysed for NO_x formation. The numerical simulations of NO_x formation were undertaken to analyse the global NO_x emissions collected from the flue gas. The strain rate was set to 100 s^{-1} in the Chemkin simulations. Although Chemkin simulation is under laminar conditions, this work focuses on the kinetic impact of the additives. It is noteworthy that the bulk flow field is consistent amongst the flame cases since the additive in the fuel mixture accounts for a small portion. The rate of production (ROP) of NO_x and its primary reaction pathways are the focus. The computational analysis provides qualitative information and insights from a chemistry aspect into the interpretation and understanding of the experimental observations.

Results and discussion

The effect of blending lower concentration biofuel surrogates (≤ 1 mol%)

Flame luminosity

The appearance and the luminosity of the turbulent non-premixed biofuel surrogate/H_2/N_2 flames are shown in Fig. 3. The mean characteristics of the flames are captured with a long exposure time of 20 s. For the 1% vapourised and sprayed toluene flames, a shorter exposure time (250 μs) is also shown to illustrate the fluctuating nature of the turbulent flames.

Fig. 3a and b shows the flame appearance of vapourised and sprayed biofuel surrogates blended H_2/N_2 flames, respectively. In Fig. 3a, a moderate effect was found on the flame volume and flame appearance of the H_2/N_2 flame from blending vapourised biofuel surrogates at 0.2 and 1 mol%. However, a clear enhancement of blue colouration was observed in the vicinity of $x/L_f = 0 - 0.5$, due to the promoted formation of CH^*, C_2^*, CO_2^* and HCO^* from blending biofuel surrogates [45,46]. In comparison to the vapourised biofuel surrogate blended flames, it is seen in Fig. 3b that changing the additives' introduction method from prevapourisation to spray solely does not achieve a highly sooting blended flame. Similar to the vapourised flames, introducing 0.2 and 1 mol% biofuel surrogates by spray has slight impacts on the flame length, width, and luminosity in comparison to the non-blended flame. It is highlighted that blending 1 mol% toluene and anisole by dilute spray (Fig. 3b) exhibits a distinct flame appearance compared with the vapourised flames (Fig. 3a). A transition of flame appearance from blue to yellow starts to take place in the 1 mol% toluene and anisole spray cases due to the soot formation. Liquid droplets in the spray flame generate local fuel-rich regions which promote soot formation, and the energy loss from the phase change in turn reduces soot oxidation. It is seen from the photographs with 20 s exposures and 1/4000 s that the soot clusters in the

vicinity of the fuel-rich region from $x/L_f = 0.4 - 0.8$. The other flame cases do not feature such a transition. Another noteworthy observation is that the spray flames display less enhancement in blue colouration near the jet exit plane between $x/L_f = 0$ and 0.4, compared with vapourised flames. This observation will be further discussed in conjunction with the signal intensity in the following paragraph.

The global signal intensity extracted from the still photographs is used to compare the luminosity of various biofuel surrogate blended flames. Fig. 4a reports the global flame luminosity extracted from the photographs, for the various fuels and introduction methods, at blending ratios of 0.2 and 1 mol%. For the 0.2 mol% blending case, it is seen that the vapourised flames display higher luminosity than the spray flames and that this is consistent for all the biofuel surrogates reported. Fig. 4b exhibits the luminosity of toluene and anisole blends as a function of flame height. It is observed in Fig. 4b that spray flames tend to have higher peak signal intensity (18% and 8% for toluene and anisole blends, respectively) than vapourised flames. The peak signal intensity appears closer to the flame tip in spray flames compared with the vapourised flames. The enhanced formation of carbon-based gaseous species accounts for the peak signal intensity observed near the jet exit in vapourised toluene and anisole flames, whereas the peak intensity in spray flames is resulting from the presence of soot. Figs. 4c and 4d show the mean flame luminosity of the vapourised/spray biofuel surrogate blended flames at $x/L_f = 0.2$ and 0.6, respectively. Vapourised biofuel surrogate blended flames show higher luminosity than spray flames at the blending ratios of 0.2 and 1 mol%, which further underpins the observation from the photographs that introducing biofuel surrogate by prevapourisation tends to have higher luminosity near the jet exit than spray. On the other hand, it is seen in Figs. 3 and 4d that as the biofuel surrogate concentration increases to 1 mol%, the luminosity of spray flames overwhelms vapourised flames at $x/L_f = 0.6$ due to the enhanced soot radiation. This luminosity difference between vapourised flames and spray flames tends to be more significant at $x/L_f = 0.2$ and less evident downstream ($x/L_f = 0.6$). The reason for the aforementioned phenomenons is that, compared with spray flames, introducing biofuel surrogates by prevapourisation facilitates the mixing between hydrogen and biofuels as phase change is avoided in such regime and the reactants actively participate in chemical reactions. Consequently, the species that contribute to the luminosity in the blue region of the flame are enhanced than in sprayed biofuel cases, as enthalpy of vapourisation is prevented.

It has been reported that prevapourised aromatic fuels are more effective than monoterpenes, and prevapourised non-oxygenated fuels are more effective than oxygenated fuels in enhancing global flame luminosity [29]. It is seen in Fig. 3a that altering the introduction method from prevapourisation to spray follows a similar trend. Sprayed aromatic biofuel surrogates (toluene and anisole) are more effective than terpene-related hydrocarbons (eucalyptol and D-limonene) in improving flame luminosity, which is consistent with the trend in vapourised flames. It is seen in Fig. 4a that blending 1 mol% toluene/anisole by spray increases the flame luminosity of the non-blended flame by 293% and 126%,

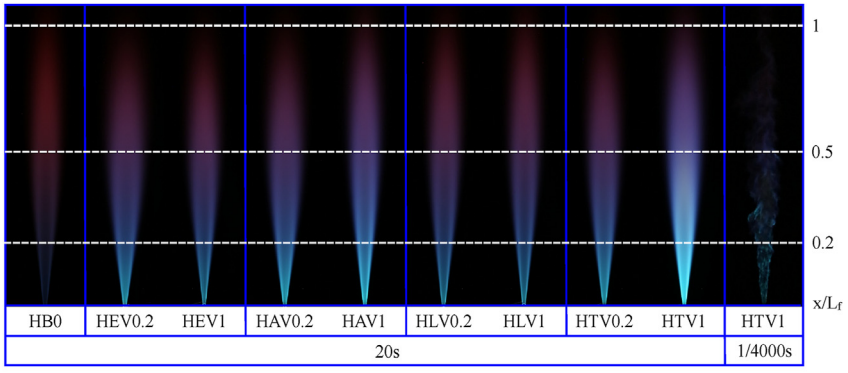

(a) Flame appearance of vapourised flames

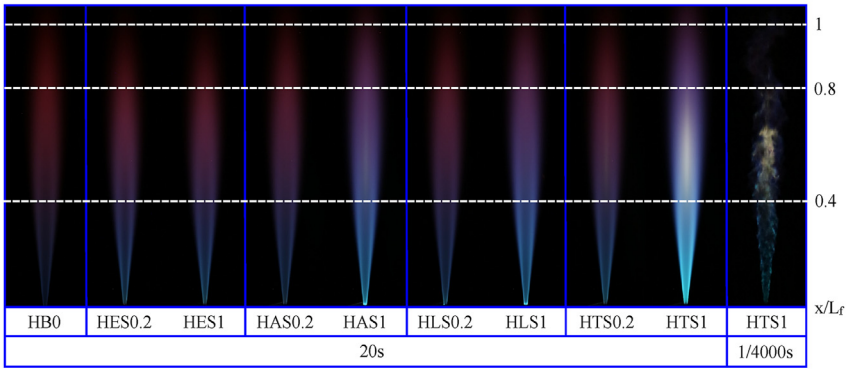

(b) Flame appearance of spray flames

Fig. 3 – Flame appearance of lower concentration (0.2 and 1 mol%) vapourised (3a) and spray (3b) biofuel surrogate/H_2/N_2 flames.

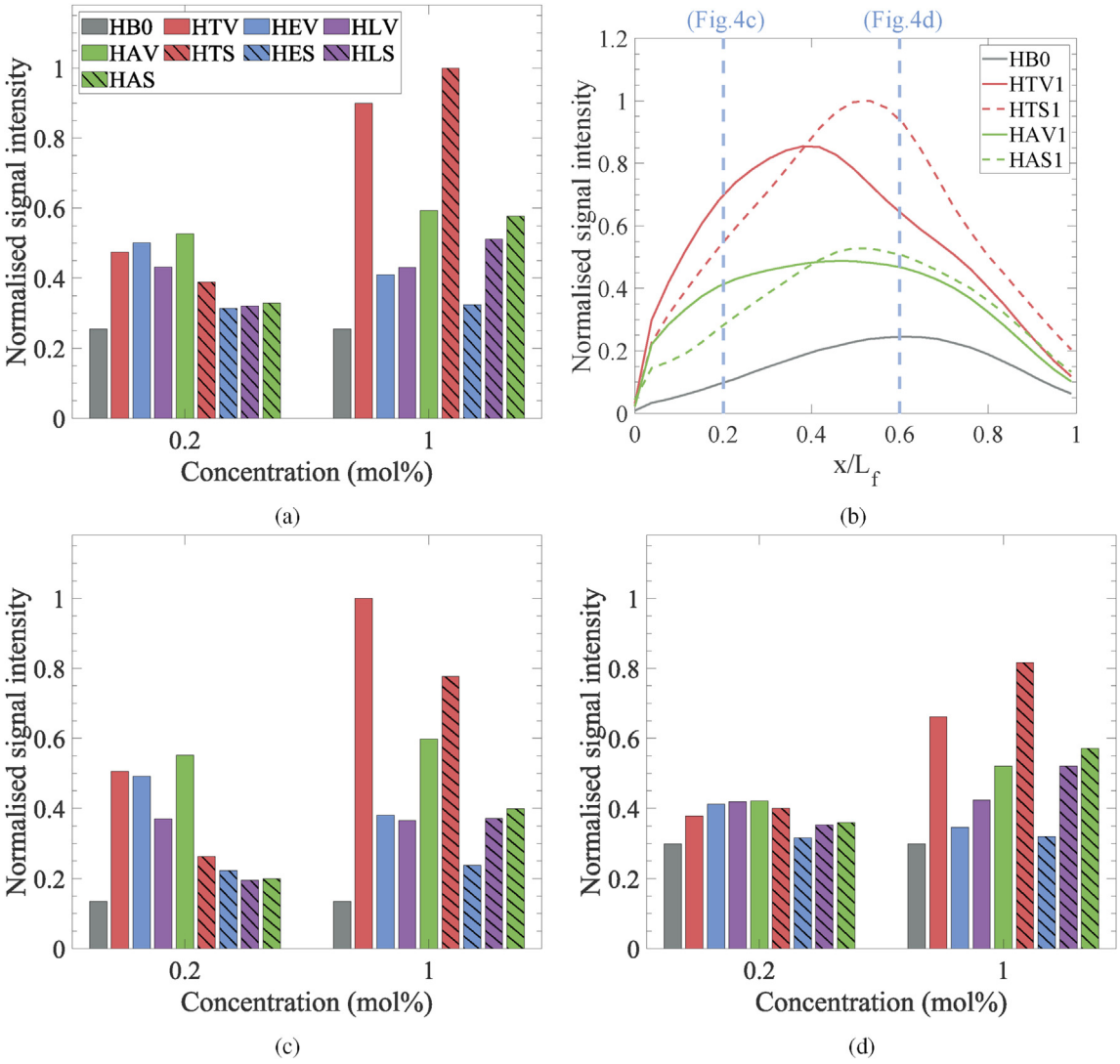

Fig. 4 – Flame luminosity of the vapourised/spray biofuel surrogate blended H_2/N_2 flames indicated by the signal intensity extracted from photographs. The signal intensity is normalised to the peak signal intensity of 1 mol% toluene spray flame. (4a) Global mean flame luminosity. (4b) Flame luminosity of toluene/anisole blends as a function of flame height. (4c) Mean flame luminosity at $x/L_f = 0.2$. (4d) Mean flame luminosity at $x/L_f = 0.6$.

respectively. Introducing 1 mol% prevapourised D-limonene and eucalyptol increases the non-blended flame by 101% and 28%, respectively. Similarly, sprayed non-oxygenated biofuel surrogates are more effective than sprayed oxygenated biofuel surrogates due to the improved soot oxidation rate from the presence of oxygen content [29]. This is also the reason for less soot being observed in the 1 mol% spray anisole flame compared with the 1 mol% toluene spray flame.

Radiant heat flux

To compare the radiant heat flux enhancement of different biofuels, the radiant fraction (χ_r) defined in Equation (2) is employed [47].

$$\chi_r = \frac{\dot{Q}_r}{\dot{Q}_F} = \frac{2\cdot\pi\cdot\left(\int_{R_0}^{R} r\cdot\dot{q}''(r)\cdot dr + R\cdot\int_{0}^{\infty}\dot{q}''(z)\cdot dz\right)}{\dot{m}\times LHV} \quad (2)$$

where χ_r is the radiant fraction, $\dot{Q}_r$ is the radiated heat (kW), and $\dot{Q}_F$ is the total thermal power (kW) of the flame. The radiated heat ($\dot{Q}_r$) in Eq. (2) is the summation of the axial (z) and radial (r) radiant heat flux ($\dot{q}''$) obtained by the heat flux transducer, R and R_0 denote the radial distance from the heat flux transducer to the centre of the nozzle exit and the flame front, respectively, $\dot{m}$ is the mass flow rate of the fuel, and LHV is the lower heating value of the fuel.

Figs. 5 and 6 show the global and axial radiant fraction, respectively, measured from non-blended and prevapourised or spray biofuel surrogate/H_2/N_2 flames. It is concluded from the results that introducing 0.2 and 1 mol% biofuel surrogate by spray is more effective than by prevapourisation in radiant intensity enhancement of H_2/N_2 flames, but the difference is not evident at lower concentration blended flames. For example, adding 1 mol% toluene by prevapourisation and

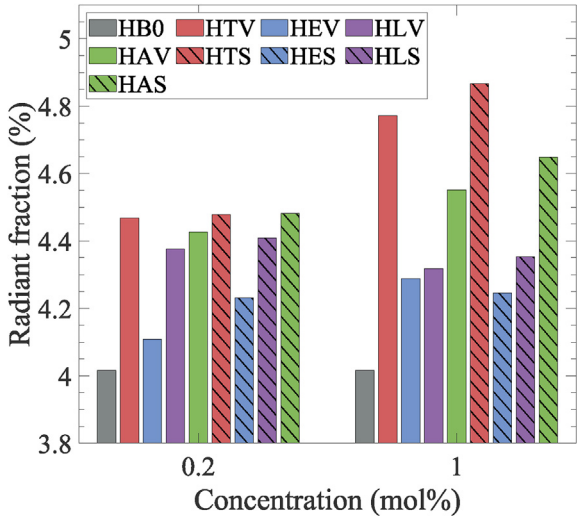

Fig. 5 – Global radiant fraction of lower concentration (0.2 and 1 mol%) vapourised/spray biofuel surrogate/H_2/N_2 flames from $x/L_f = 0 - 0.4$.

spray increases the radiant fraction (χ_r) of the HB0 flame by 18% and 22%, respectively. Adding 1 mol% anisole by prevapourisation increases the radiant fraction of the HB0 flame by 13%, compared with a 16% increase from the spray. It is also found that introducing the additives by spray instead of prevapourisation has a larger impact on the radiant fraction enhancement of the 1 mol% toluene and anisole blends than other biofuel surrogate blended flames. This phenomenon can be correlated to the observation in Section Flame luminosity that soot formation is promoted in these two flame cases directly as a result of changing the introduction method.

The results from Figs. 5 and 6 indicate that blending lower concentration biofuel surrogates to a H_2/N_2 flame by spray has a limited impact on radiant heat flux enhancement. It was concluded in Section Flame luminosity that changing the introduction method from prevapourisation to spray does not attain a highly sooting flame at 0.2 and 1 mol% additive concentration, therefore, the source of radiative heat transfer from these lower concentration biofuel blended flames is still from gaseous species (e.g., CO, CO_2, and H_2O). It is known that gaseous species have much less radiant heat flux than soot at

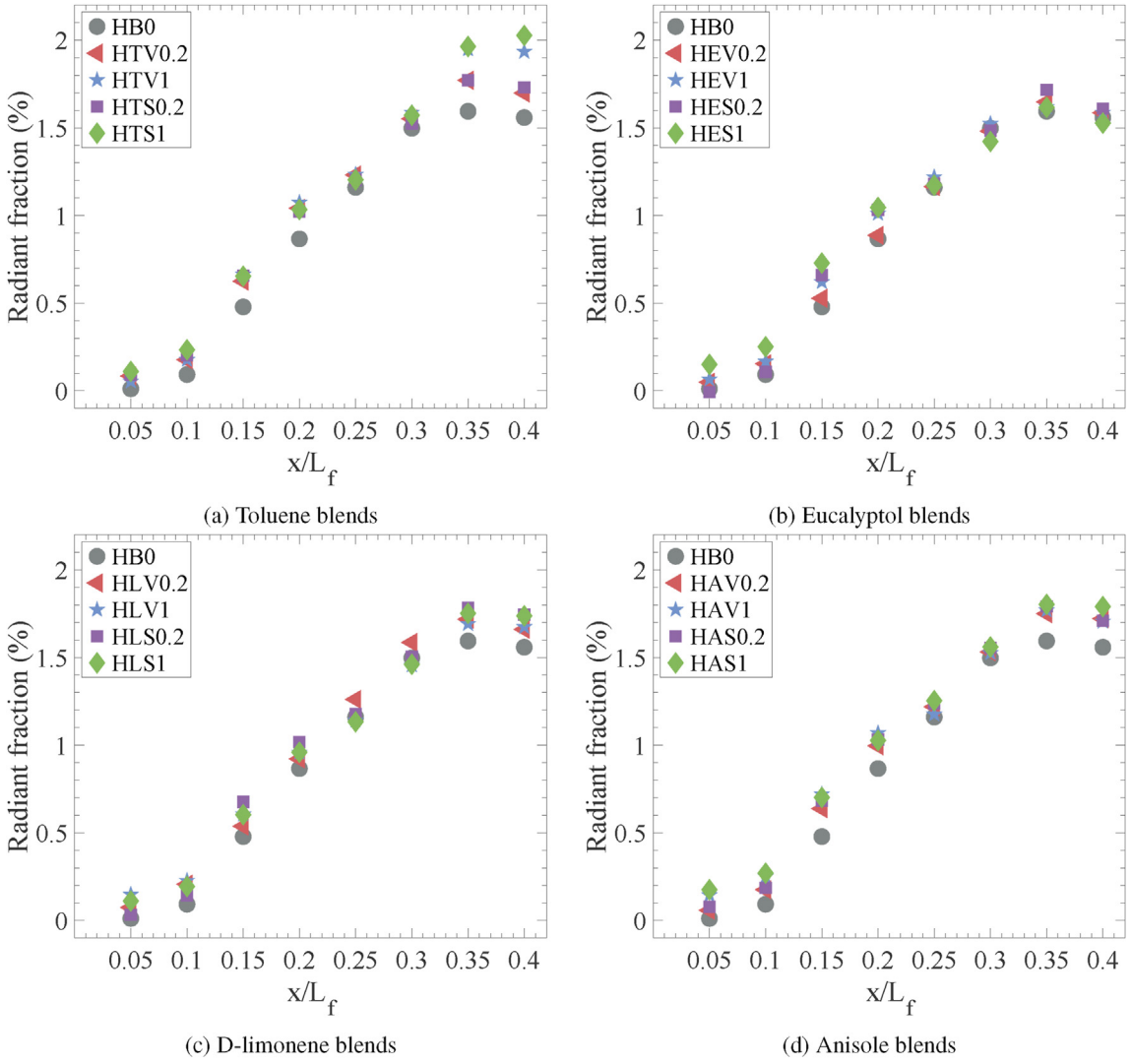

Fig. 6 – Axial radiant fraction of lower concentration (0.2 and 1 mol%) vapourised/spray biofuel surrogate/H_2/N_2 flames described in Table 1.

equivalent temperature [48]. Another factor that contributes to the limited radiant intensity enhancement observed in the 9:1 mol H_2/N_2 flame is that such flame with high hydrogen concentration has abundant OH radicals and high flame temperature, leading to a high oxidation rate that hampers sooting formation from the relatively low carbon flux (note that the concentration of carbon atoms in lower concentration biofuel blended flames are about $0.02-0.07$, much lower than conventional hydrocarbon fuels). Therefore, an additional flame case with lower hydrogen concentration was tested to evaluate the effect of hydrogen concentration on the flame characteristics of biofuel surrogate blended H_2/N_2 flames. The results will be further discussed in Section The effect of blending higher concentration vapourised toluene ($\geq$ 3.5mol %).

It is observed in Fig. 6 that the radiant fraction of spray toluene and anisole blended flames reach the peak value at $x/L_f = 0.4$ between $x/L_f = 0-0.4$, which is dissimilar to the trend in other vapourised/spray biofuel-blended cases — reaches the peak radiant fraction at $x/L_f = 0.35$. In the flames without soot (i.e., all flame cases except for 1 mol% spray toluene/anisole flames), the flame luminosity and radiant fraction reach their peaks closer to the jet exit as a result of enhanced formation of gaseous species. On the other hand, in the 1 mol % spray toluene and anisole blended flames where soot formation becomes evident from $x/L_f = 0.4$, soot loading is the major contributing factor to the radiant intensity enhancement. This finding is consistent with the observations in Fig. 4.

Another noteworthy finding in Fig. 5 is that the global radiant fraction from $x/L_f = 0-0.4$ of the spray D-limonene blended flame case shows a decreasing trend with the increase in additive concentration, indicating that other factors may play important roles in radiant intensity enhancement in addition to carbon flux. Introducing 0.2 mol% D-limonene as a spray enhances the radiant fraction of the HB0 flame by 10%, but adding 1 mol% spray D-limonene enhances the radiant fraction by 8%. It was reported that flame temperature is one of the contributing factors to the radiant heat flux as the flame's radiated heat is proportional to the fourth power of temperature — $Q_r \propto T^4$ [29]. The impact is more evident in spray flames The spray flame temperature results presented in Section 3.1.3 further support this finding.

Flame temperature

Fig. 7 reports the mean axial flame temperature along the centreline for both the vapourised and spray biofuel surrogate blended H_2/N_2 flames. The results show that introducing prevapourised biofuel surrogates increases the mean centreline flame temperature of the non-blended H_2/N_2 flame near the jet exit plane while decreasing the flame temperature at the region further into the momentum-driven part. Compared with vapourised flames, adding biofuel surrogates to HB0 flames by spray evidently decreases centreline flame temperature. The most significant reduction is recorded to be 213 K in 1 mol% spray D-limonene blends at $x/L_f = 0.05$. Dissimilar to the trend of all vapourised flame cases, reductions in mean centreline flame temperature are observed throughout the flame from $x/L_f = 0.05-0.4$ in spray flames.

It is seen in Fig. 7 that spray flames generally have lower mean centreline flame temperature than vapourised or non-blended flame, particularly near the exit plane. The enthalpy of vapourisation leads to a reduction in the temperature of the spray flames. The temperature difference tends to be less downstream, where the rate of vapourisation decreases. The prevapourised biofuel surrogates and hydrogen mixture actively participate in the reactions mixed with oxidant when they leave the jet exit, while sprayed biofuel surrogates first require energy for phase change. Therefore, a faster and more homogeneous mixing is achieved in vapourised flames and subsequently results in higher flame temperature. It was discussed in Sections Flame luminosity and Radiant heat flux that in these lower concentration biofuel surrogate blended flames, where thermal radiation is primarily from gaseous species, higher flame temperature and higher heat release rate lead to higher flame luminosity and radiant intensity. The mean flame temperature results further provide evidence to explain why all vapourised flames display higher flame luminosity at $x/L_f = 0.2$ in Fig. 4b and reach their peak luminosity closer to the jet exit plane in Fig. 4d, compared with spray flames. Temperature reduction is the reason that radiant fraction decreases with the increase in biofuel concentration (i.e., carbon flux). The largest temperature reduction (ie., 213 K in 1 mol% spray D-limonene) is correlated to the lower radiant fraction in 1 mol% spray D-limonene blends, compared with 0.2 mol% spray D-limonene blends (discussed in section Radiant heat flux).

Large mean centreline flame temperature drops are also observed in 1 mol% spray toluene and anisole blends (Figs. 7a and d), however, exhibiting an opposite trend to D-limonene blends regarding radiant heat flux. Soot formation becomes evident in the 1 mol% spray toluene and anisole blended flame, hence the source of the radiative heat transfer in these flames gradually shifts from gaseous species to a stronger source — soot. It is known that lower temperature favours soot formation since the soot oxidation rate is reduced [15,49]. Therefore, the reduced mean flame temperature in the 1 mol% spray toluene blends and anisole blends contributes to soot formation and subsequently results in laser radiant fraction increases. It is also observed in Fig. 7a that 1 mol% spray toluene blends and anisole blends see larger mean temperature drops in the vicinity of $x/L_f = 0.3$ compared with D-limonene and eucalyptol. In addition to the enthalpy of vapourisation of liquid droplets in spray flames, it is also ascribed to the elevated radiative heat loss from the soot, which is consistent with the observation in spray flame photographs (Fig. 3b) that soot loading becomes evident in 1 mol% spray anisole and toluene-blended flames. This phenomenon will be further demonstrated in Section The effect of blending higher concentration vapourised toluene ($\geq$ 3.5mol%).

NO_x emissions

The emission index for NO_x (EI_{NO_x}) is calculated using Eq. (3) [50,51]:

$$EI_{NO_x} = \frac{X_{NO_x}}{(X_{CO} + (X_{CO_2} - X_{CO_{2amb}}))} \times \frac{n_c \times MW_{NO_x}}{MW_f \times LHV_f} \quad (3)$$

where X denotes the mole concentration of NO_x, CO, CO_2 in the flue gases, CO_{2amb} is the mole fraction of CO_2 in ambient air, n_c is the carbon concentration of fuel, MW_{NO_x} is the

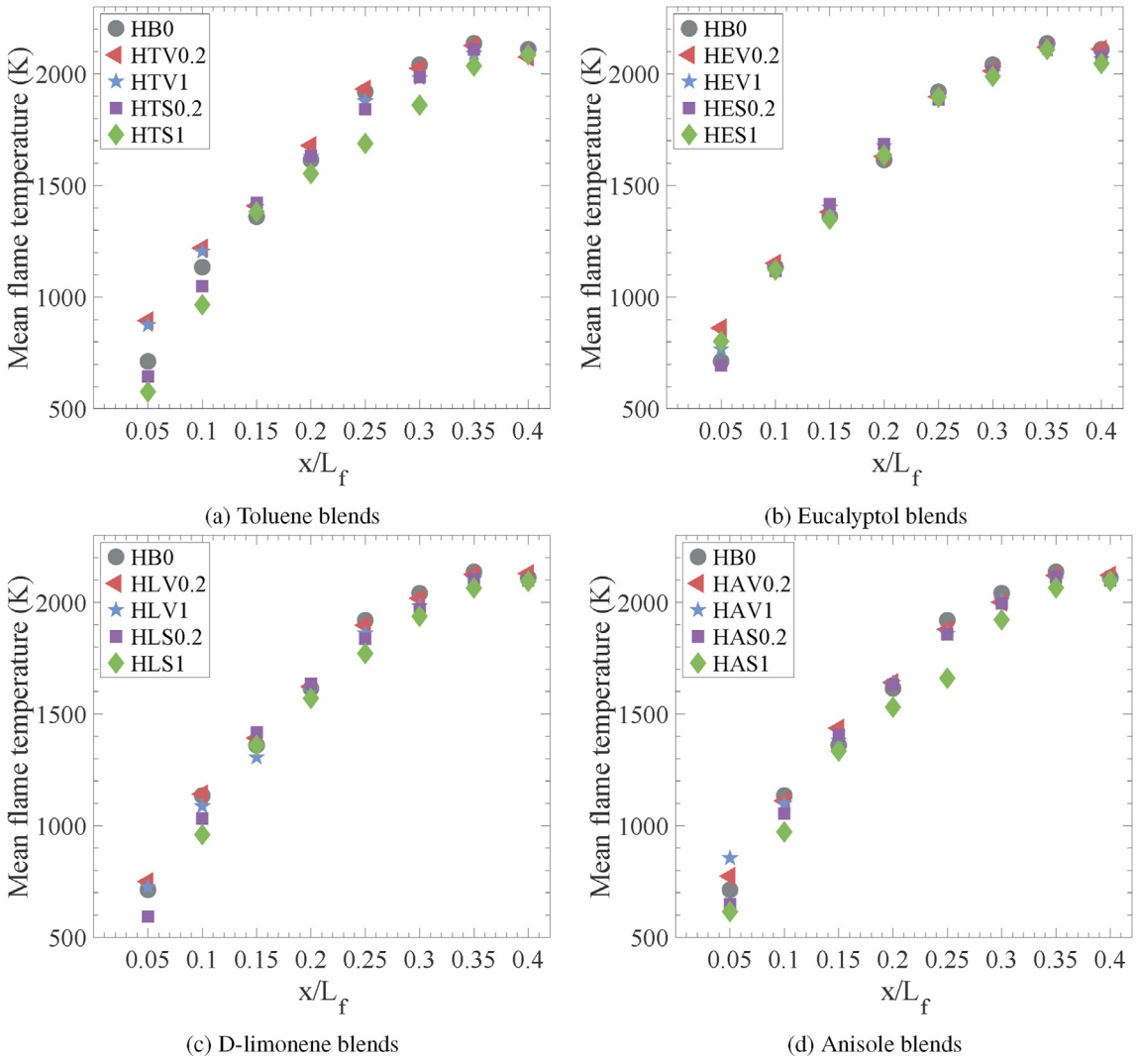

Fig. 7 – Mean axial flame temperature along the centreline of lower concentration (0.2 and 1 mol%) vapourised/spray biofuel surrogate/H_2/N_2 flames described in Table 1. The results are corrected for radiative heat loss from the thermocouple.

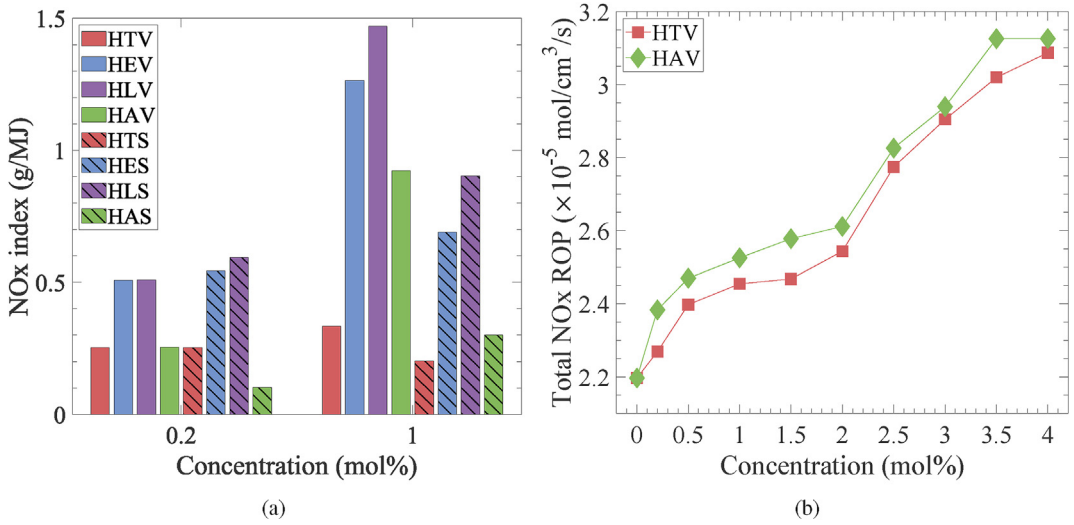

Fig. 8 – Global NO_x emissions measured in the experiment and numerical simulation of NO of lower concentration (0.2 and 1 mol%) vapourised/spray biofuel surrogate/H_2/N_2 flames described in Table 1. (8a) Emission index for NO_x measured in the experiment. (8b) ROP of NO in toluene and anisole blends from numerical simulation.

molecular weight of NO_x, MW_f and LHV_f denote the molecular weight and the lower heating value of the fuel mixture, respectively. Note that Eq. (3) is not applicable to carbon-free fuel mixtures [51].

The EI_{NO_x} (g/MJ) from measurements in both the spray and vapourised biofuel surrogate blended H_2/N_2 flames is plotted as a function of biofuel concentration in Fig. 8a. Fig. 8b presents the total ROP of NO_x in toluene and anisole blends as a function of concentration from numerical modelling. The results show that introducing 1 mol% additives into the H_2/N_2 flames by spray results in lower EI_{NO_x} than introducing prevapourised biofuel surrogates. Introducing 0.2 and 1 mol% anisole by spray decreases the EI_{NO_x} by 60% and 67%, respectively, compared with introducing 0.2 and 1 mol% anisole by prevapourisation. This is mainly because the lower centreline flame temperature (Fig. 7) measured in spray flames reduces NO_x formation via the thermal route. Thermal NO_x was previously reported as the dominant NO_x formation route in hydrogen-based flames [52,53].

It is highlighted in Fig. 8 that as the biofuel surrogate concentration increases from 0.2 mol% to 1 mol%, the EI_{NO_x} increases. However, the centreline flame temperature shown in Fig. 7 does not exhibit a positive correlation with biofuel surrogate concentration in vapourised flames. Furthermore, the numerical results from the OPPDIF simulation in Fig. 9 show that as the biofuel surrogate concentration increases, the peak adiabatic flame temperature of vapourised toluene and anisole blended flames decreases from 2302 K to 2238 K, while the total NO_x ROP in Fig. 8b displays an increasing trend. These observations imply that other NO_x formation pathways in addition to the thermal route may enhance NO_x formation in biofuel surrogate blended flames. Therefore, a detailed modelling of NO_x formation reaction pathways was conducted.

Nitrogen oxides (NO_x) is predominantly comprised of nitric oxide (NO) with a minor proportion of nitrogen dioxide (NO_2). It is found in the simulation that the ROP of NO_2 is two orders of magnitude smaller than that of NO. Thus, the computational analysis is focused on the reaction pathways of NO. Fig. 10 presents the ROP for four primary reaction pathways of NO — three NO formation pathways and one consumption

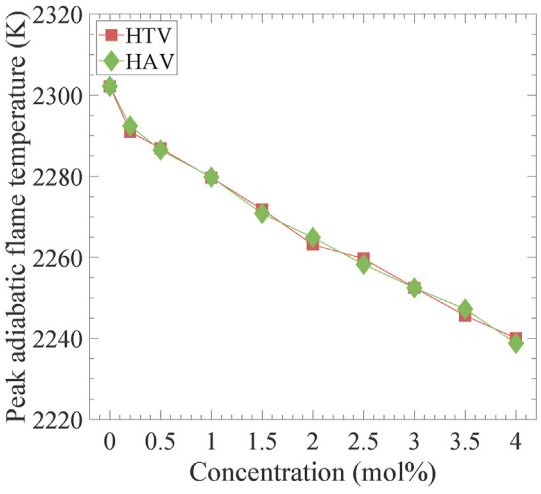

Fig. 9 – Peak adiabatic flame temperature of toluene and anisole blends from numerical simulation.

pathway. It is seen from Fig. 10a that the ROP of NO via the $OH + N \rightleftharpoons H + NO$ reaction increases with the vapourised toluene and anisole addition. This reaction pathway is known as one of the subsets in the thermal NO formation route [30]; however, it does not mean this reaction is driven by the flame temperature. It is the first reaction in the thermal route: $O + N_2 \rightleftharpoons NO + N$ that requires high energy from the flame temperature and initiates the NO formation. This reaction also controls the reaction rate via the thermal route [30]. Based on this understanding, the acceleration of NO formation via the $OH + N \rightleftharpoons H + NO$ reaction in these biofuel surrogate blended H_2/N_2 flames likely results from the OH and N radical increase. The OH radicals are expected to be abundant in hydrogen-based flames. The N radicals, on the other hand, are usually created from CH_i radicals attacking the triple bond in N_2 [54]. Therefore, as the concentration of CH_i radicals increases with the biofuel surrogate addition, the production of N radicals is subsequently promoted and hence leads to the increase in NO formation. The CH_i radicals are also involved with the reaction pathways associated with prompt NO formation, which will be discussed in the following paragraph.

The prompt route is another reaction pathway that is expected to have a major effect on the NO formation. The prompt route is initiated by $CH + N_2 \rightleftharpoons H + NCN$ and then the NCN radical forms HCN via the $NCN + H \rightleftharpoons HCN + N$ reaction. The HCN radical subsequently reacts with O to eventually form NO. It is noted in Fig. 10b that the prompt NO_x formation route is of less importance in lower concentration (0.2 and 1 mol%) vapourised biofuel surrogate blended flames, which is an order of magnitude smaller than the $OH + N \rightleftharpoons H + NO$ route.

Fig. 10c indicates that HNO plays an important role in NO formation via the $H + HNO \rightleftharpoons H_2 + NO$ reaction, which is known as the HNO-intermediate route [55]. The ROP of NO via this route tends to decrease with the increase in biofuel surrogate concentration. To investigate the reason behind this trend, the reaction chain of HNO needs to be understood. HNO is generally formed from NH through $NH + OH \rightleftharpoons HNO + H$ reaction, and the formation of NH is related to the subset of NNH route: $NNH + O \rightleftharpoons NO + NH$. The NNH route emphasises the influence of H and O radicals at flame fronts and rich regions, especially in hydrogen flames [52]. The oxygen content in anisole actively participates in the $NNH + O \rightleftharpoons NO + NH$ reaction and hence results in a slower decrease in NO formation via the HNO-intermediate route than toluene.

The process of NO consumption to a relatively steady state N_2 is another important consideration. Fig. 10d shows the ROP of NO consumed to N_2 via the $NO + N \rightleftharpoons N_2 + O$. Higher ROP is observed in the H_2/N_2 flame without biofuel surrogate, which in turn results in more NO formation in biofuel-blended flames. Combined with the ROP of other major reaction pathways, the overall ROP of NO tends to increase with the biofuel surrogate addition, which agrees with the experimental results in Fig. 8a.

Another noteworthy observation from both experimental and numerical results is that vapourised anisole tends to produce more NO_x than vapourised toluene at low concentrations. It is seen from Figs. 8 and 10 that the differences of NO ROP along with the NO consumption rate between anisole

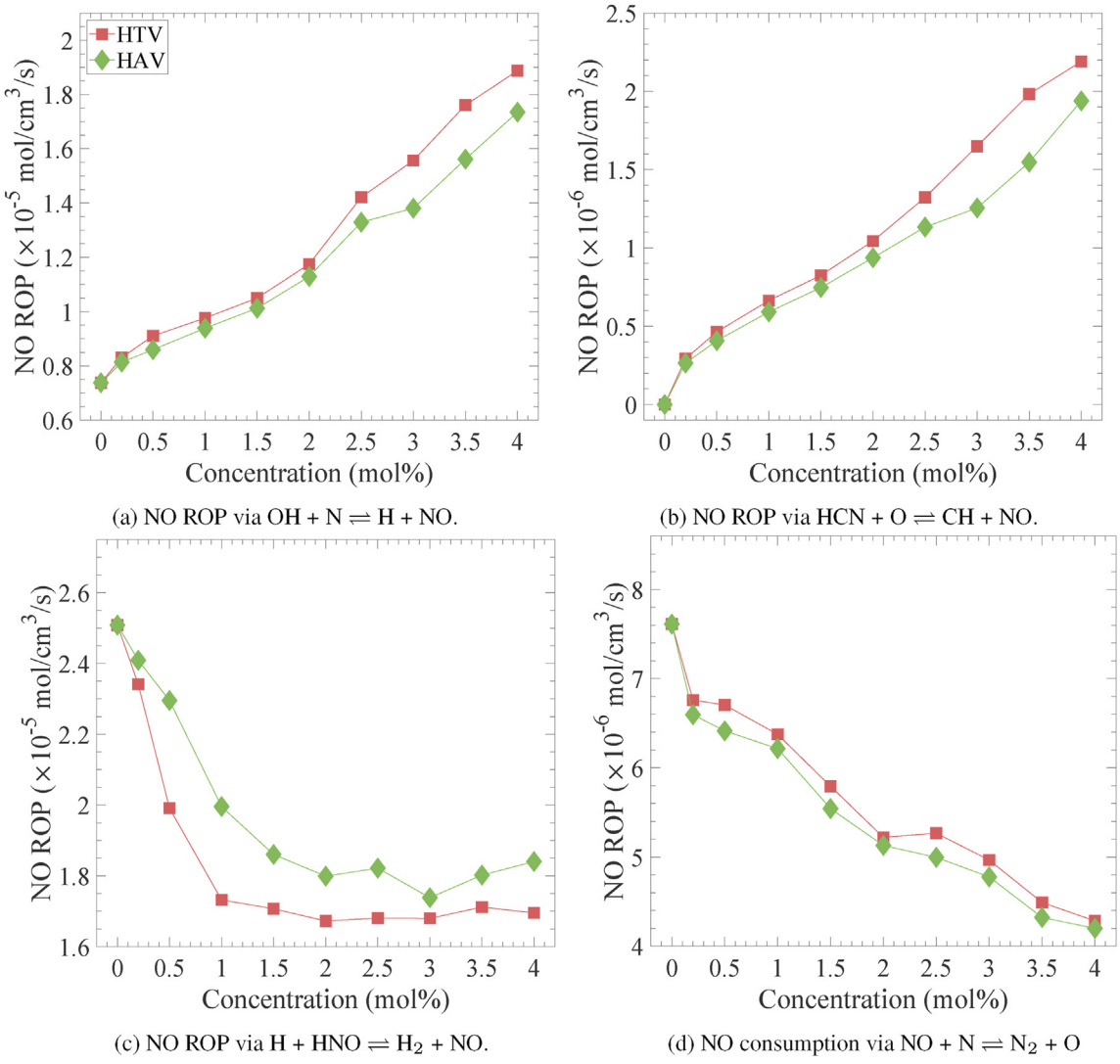

Fig. 10 – Reaction pathways of NO in toluene and anisole blends from numerical modelling.

and toluene via the OH + N ⇌ H + NO, NO + N ⇌ N_2 + O, and HCN + O ⇌ CH + NO routes are minor compared with the most distinct difference via the HNO-intermediate route: H + HNO ⇌ H_2 + NO. This is because the weak chemical bond in anisole chemical structure, which connects the oxygen atom and aromatic ring, is easily broken to form free oxygen atoms which then actively participate in the NNH route through NNH + O ⇌ NO + NH reaction to form NH and hence HNO [56].

It is seen in Fig. 8a that cyclic monoterpene biofuels (eucalyptol and D-limonene) generally have higher EI_{NO_x} compared with toluene and anisole. Furthermore, the EI_{NO_x} of 0.2 and 1 mol% D-limonene blends is higher than that of eucalyptol-blended flames, either by spray or prevapourisation. D-limonene is a non-oxygenated fuel that is comprised of a C=C double bond, while eucalyptol is an oxygenated fuel without C=C double bonds. Previous studies show that the presence of C=C double bond and oxygen content in the chemical structure of a fuel increase the flame temperature and lead to higher NO_x emissions [57,58]. The EI_{NO_x} comparison between D-limonene and eucalyptol may imply that the effect of unsaturation degree on NO_x emissions is more significant than the oxygen content in these biofuel surrogate blended H_2/N_2 flames.

The effect of blending higher concentration vapourised toluene ($\geq$ 3.5 *mol%*)

Higher concentrations (3.5 and 4 mol%) of vapourised toluene are blended in H_2/N_2 flames to investigate the combustion characteristics and compare them with the lower concentration cases. As discussed in Section The effect of blending lower concentration biofuel surrogates ($\leq$ 1 mol%), high hydrogen concentration can be a major factor that hampers soot formation. Therefore, an additional 3.5 mol% vapourised toluene-blended H_2/N_2 (7:3 by mole) flame case (LHTV3.5) with U/d = 12,800 s^{-1} was tested. In this section, the flame appearance, radiant fraction, centreline flame temperature, and NO_x emission of the LHTV3.5 flame are presented to evaluate the effect of lower exit strain rate, H_2 and N_2 concentration on flame characteristics.

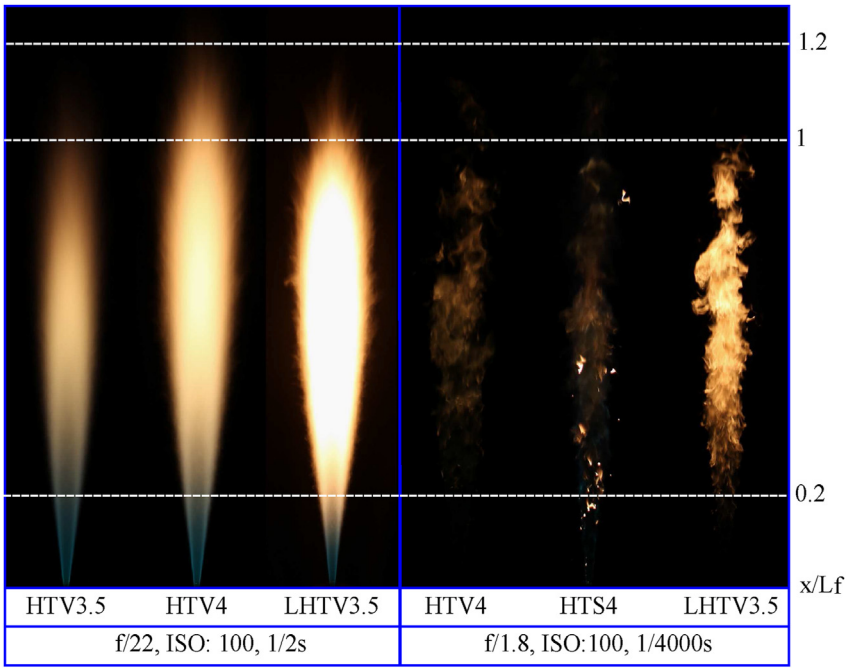

Fig. 11 – Photographs of 3.5 and 4 mol% vapourised toluene-blended H_2/N_2 flames (HTV3.5 and HTV4) and the 3.5 mol% vapourised toluene-blended H_2/N_2 flame with lower hydrogen concentration (LHTV3.5) described in Table 1.

Fig. 11 presents photographs of the flame appearance with longer (0.5 s) and shorter exposure times (250 μs). There is a clear transition from blue to yellow colouration as the vapourised toluene concentration increases from 0.2 to 3.5 mol%, which indicates that soot is markedly promoted. The blue colouration, which represents the gaseous species as discussed in Section Flame luminosity, is distributed near the exit plane ($x/L_f \leq 0.2$), but the length of this region becomes shorter as the toluene concentration further increases. The photographs with shorter exposure times (250 μs) capture the instantaneous distribution of soot in flames. Soot is predominantly distributed between $x/L_f = 0.2 - 0.8$ and its chaotic state is because of flame turbulence. The photograph of the 4 mol% spray toluene blended flame is presented to show the visual observation of toluene droplets burning in the flame. The local fuel-rich condition created by toluene droplets significantly enhances soot formation near that region. This characteristic of spray flame is distinct from the vapourised flame and it is the major contributing factor to the difference between 1 mol% vapourised/spray toluene and anisole flames in Fig. 3. Fig. 12a provides signal intensity extracted from the photograph to demonstrate the luminosity enhancement of 3.5 mol% toluene. The signal intensity of the 3.5 mol% toluene flame is 34 times greater than the 1 mol% toluene flame, and this value is more than doubled at 4 mol% (70 times).

Fig. 12b shows the radiant fraction measured from the 0, 3.5, and 4 mol% vapourised toluene blends. Unlike lower concentration biofuel-blended flames, blending high concentration toluene to H_2/N_2 flame tends to have a larger non-linear increase in radiant fraction starting from $x/L_f = 0.35$. At $x/L_f = 0.4$, increasing the vapourised toluene concentration to 4 mol% leads to a 33% increase in the radiant fraction of the HB0 flame, compared with 21% increase by blending 1 mol% vapourised toluene. The radiant fraction of the 4 mol vapourised toluene is increased by 52% compared with the non-blended H_2/N_2 flame. The previously reported numerical results of naphthalene ROP have further underpinned the experimental observation [29]. The formation of naphthalene in lower concentration (0 – 2 mol%) toluene and anisole blends is moderate, followed by a large non-linear increase as the biofuel concentration rises from 2 to 4 mol%. This further supports the finding that blending lower concentrations of biofuels has limited impact on the flame appearance and radiant fraction of a H_2/N_2 flame, but a clear transition in flame appearance and the radiant fraction is observed when blending higher concentration biofuels.

Fig. 12c shows the mean axial flame temperature along the centreline of higher concentration toluene blended H_2/N_2 flames. It is seen from Fig. 12c that the overall trend of mean centreline flame temperature variation in higher concentration vapourised toluene blends is dissimilar to the lower concentration vapourised cases — the mean centreline flame temperature displays a decreasing trend starting from $x/L_f = 0.25$, which is not seen in the lower concentration vapourised biofuel surrogate blended flames, but only in spray flames. It was discussed in Section Flame temperature that the reduced mean centreline flame temperature in spray flames is due to the enthalpy of vapourisation of liquid droplets, which does not occur in the prevapourised flames. In conjunction with the radiant fraction results in Fig. 12b, the reduced mean centreline flame temperature found in the higher concentration vapourised toluene blended flame (HTV3.5 and 4) is due to the increased radiative heat loss from the soot enhancement. The reduced mean flame temperature in these flames leads to a lower soot oxidation rate, which further promotes the soot production in the flame.

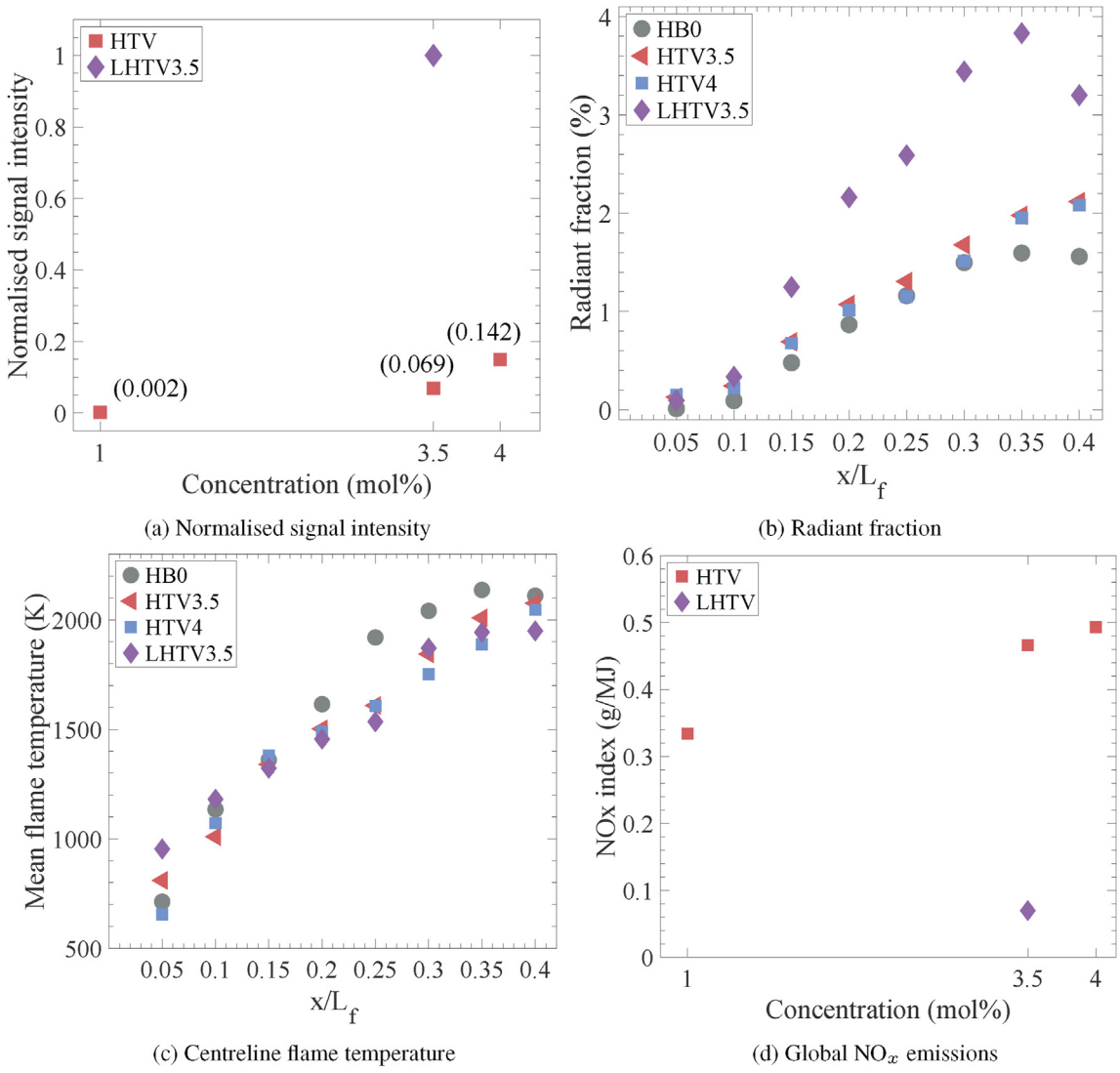

Fig. 12 – Flame characteristics of vapourised toluene-blended H_2/N_2 flames (HTV1, HTV3.5 and HTV4) and the 3.5 mol% vapourised toluene-blended H_2/N_2 flame with lower hydrogen concentration (LHTV3.5) described in Table 1. (12a) Normalised signal intensity from photographs. The signal intensity is normalised to the peak signal intensity among the vapourised toluene flames. (12b) Radiant fraction from $x/L_f = 0.05 - 0.4$. (12c) Mean axial flame temperature along the centreline of the flames. The results are corrected for radiative heat loss from the thermocouple. (12d) Global NO_x emissions.

Fig. 12d reports the global EI_{NO_x} of higher concentration vapourised toluene-blended H_2/N_2 flames. The emission index for NO_x increases by 40% from 1 to 3.5 mol% vapourised toluene blends, and further increases by 6% from 3.5 to 4 mol%. The increasing trend of EI_{NO_x} in higher concentration vapourised toluene blends is consistent with the lower concentration cases discussed in Section NOx emissions. As is shown in Fig. 8, the kinetic mechanism and dominating reaction pathways of NO formation in 3.5 and 4 mol% vapourised toluene blends are not dissimilar to the lower concentration cases, with one distinct exception that the ROP of NO formation through prompt route: $HCN + O \rightleftharpoons CH + NO$ reaction in 4 mol% toluene blends is 7 times greater than that in 0.2 mol% toluene blends. This implies that as the toluene concentration increases to 4 mol%, HCN radicals formed from CH and NCN routes are enhanced. Hence, NO formation through the prompt route has gradually become one of the primary reaction pathways in higher concentration toluene-blended H_2/N_2 flames.

As discussed in Section Introduction, adding hydrogen to hydrocarbon fuels reduces soot loading of the flame via three mechanisms: thermal effect, dilution effect, and chemical effect [11–13,16,59]. Therefore, an additional 7:3 H_2/N_2 flame case with lower hydrogen concentration, blended with 3.5 mol % vapourised toluene (LHTV3.5) was tested (see flame details in Table 1). It is also noted that the exit strain rate of the higher hydrogen concentration flame cases is above 20,000 s^{-1}, whereas the lower hydrogen flame case is only 12,800 s^{-1}. A high exit strain rate (low residence time) is known to inhibit soot formation as the key soot formation processes — surface growth and agglomeration require time [60]. The flame luminosity, radiant fraction, centreline flame temperature, and NO_x emission of the lower H_2 concentration flame (LHTV3.5) are presented in the figures along with the higher H_2

concentration flame (HTV3.5) for comparison. The signal intensity which indicated the flame luminosity in Fig. 11 shows that the 3.5% vapourised toluene-blended flame with low hydrogen concentration (LHTV3.5) is 15 times greater than the 3.5 mol% vapourised toluene blends with higher hydrogen concentration (HTV3.5). For radiant fraction enhancement, it is seen in Fig. 12b that the radiant fraction of the 3.5 mol% vapourised toluene blends with lower hydrogen concentration (LHTV3.5) increases the radiant fraction of the HB0 flame by 135% at $x/L_f = 0.35$. The results demonstrate the significant enhancement of flame luminosity and radiant intensity of the non-blended H_2/N_2 flame from reducing the hydrogen concentration with constant bulk mean Reynolds number and toluene concentration. Additionally, the global NO_x emissions (Fig. 12d) decrease by 68% compared with the high hydrogen concentration 3.5% toluene blends. The reduced temperature inhibits the NO formation via the thermal route and the reduced H_2 concentration results in lesser H and OH radicals, which in turn inhibits the reaction pathways via the $OH + N \rightleftharpoons H + NO$ and $H + HNO \rightleftharpoons H_2 + NO$ routes.

Conclusions

The effect of biofuel blending with H_2/N_2 turbulent non-premixed jet flames was investigated in this study. Both vapourised and sprayed biofuel surrogates are used and the flames' appearance, flame luminosity, radiant intensity, centreline flame temperature, and NO_x emissions are investigated through combined experimental and numerical methods. Based on experimental observations and numerical results, the following conclusions are made:

1. Soot starts to form in the 1 mol% spray toluene and anisole blends between $x/L_f = 0.4 - 0.8$. Blending higher concentrations (3.5 and 4 mol%) vapourised toluene to H_2/N_2 flames results in a clear transition into a sooting flame. The flame luminosity of the 3.5 mol% toluene flame is 34 times greater than the 1 mol% toluene flame. The radiant fraction of the 4 mol% vapourised toluene flame at $x/L_f = 0.4$ is increased by 33% compared with the 1 mol% toluene flame.
2. Introducing biofuel surrogates in liquid droplets to H_2/N_2 flames has demonstrated its advantages in promoting soot formation by creating a local fuel-rich condition. Vapourised flames are more luminous and display a higher radiant fraction near the jet exit as the vapourised biofuels facilitate the mixing with H_2 and actively participate in the oxidation reactions, while sprayed biofuel surrogates first require energy for phase change. The centreline flame temperature in spray flames is lower due to the enthalpy of vapourisation, which in turn favours the formation of soot precursors. The NO_x emission from 1 mol% spray biofuel surrogate blended flames is lower than vapourised flames since the lower temperature in spray flames reduces thermal NO_x formation.
3. Both experimental and numerical results show that the global NO_x emissions from the turbulent nonpremixed H_2/N_2 flame increase with biofuel surrogate addition. The numerical simulation shows that the primary NO formation reaction pathways are the subset of the thermal route: $OH + N \rightleftharpoons H + NO$ and prompt route: $CH + N_2 \rightleftharpoons H + NCN$, with HNO-intermediate route: $H + HNO \rightleftharpoons H_2 + NO$ also contributing. The addition of biofuel surrogates mainly enhances NO_x formation via thermal and prompt routes, leading to the increase in global NO_x emission.
4. High hydrogen concentration of the turbulent non-premixed hydrogen-based flames has a major inhibition effect on soot formation and corresponding radiative heat flux. As the hydrogen concentration decreases from 90% to 70% in the H_2/N_2 mixture, while Reynolds number (10,000) and toluene concentration (3.5 mol%) are kept constant, the radiant fraction of the LHTV3.5 flame is increased by 115% at $x/L_f = 0.35$, compared with the HTV3.5 flame. The global NO_x emissions of the LHTV3.5 flame case decrease by 68% compared with the HTV3.5 flame case. The global NO_x emissions from both the LHTV3.5 and HTV3.5 flame cases are lower than the non-blended H_2/N_2 (HB0) flame case. The elevated radiative heat loss reduces the flame temperature in the LHTV3.5 flame case, which in turn inhibits the NO formation via the thermal route.

The key findings in this paper further contribute to the understanding of biofuel-blended hydrogen flames, revealing that hydrogen concentration in the fuel mixture and exit strain rate may be dominating in enhancing flame luminosity and radiant heat flux, compared with other factors (e.g., the chemical structure of additive). It is also highlighted that the NO_x emissions increase with biofuel addition via the subset of the thermal route and prompt route, which is another potential challenge in evaluating the feasibility of biofuel-blended hydrogen flames.

Declaration of competing interest

The authors declare that they have no known competing financial interests or personal relationships that could have appeared to influence the work reported in this paper.

Acknowledgements

The research reported in this publication was supported by funding from the University of Adelaide, the Australian Research Council (ARC), and the Future Fuels Cooperative Research Centre (CRC). The assistance with the experimental work from Jason Peak, Kae Ken Foo, Adam John Gee, and Douglas Proud is acknowledged.

REFERENCES

[1] Dodds PE, Staffell I, Hawkes AD, Li F, Grünewald P, McDowall W, et al. Hydrogen and fuel cell technologies for heating: a review. Int J Hydrogen Energy 2015;40:2065–83.
[2] Kitagawa T, Nakahara T, Maruyama K, Kado K, Hayakawa A, Kobayashi S. Turbulent burning velocity of hydrogen–air premixed propagating flames at elevated pressures. Int J Hydrogen Energy 2008;33:5842–9.

[3] Nag S, Sharma P, Gupta A, Dhar A. Experimental study of engine performance and emissions for hydrogen diesel dual fuel engine with exhaust gas recirculation. Int J Hydrogen Energy 2019;44:12163–75.
[4] Nowotny J, Veziroglu TN. Impact of hydrogen on the environment. Int J Hydrogen Energy 2011;36:13218–24.
[5] Yuan C, Han C, Liu Y, He Y, Shao Y, Jian X. Effect of hydrogen addition on the combustion and emission of a diesel free-piston engine. Int J Hydrogen Energy 2018;43:13583–93.
[6] Akal D, Öztuna S, Büyükakın MK. A review of hydrogen usage in internal combustion engines (gasoline-Lpg-diesel) from combustion performance aspect. Int J Hydrogen Energy 2020;45:35257–68.
[7] Kanth S, Debbarma S, Das B. Experimental investigations on the effect of fuel injection parameters on diesel engine fuelled with biodiesel blend in diesel with hydrogen enrichment. Int J Hydrogen Energy 2022;47:35468–83.
[8] Gürbüz H. Analysis of the effects of multiple injection strategies with hydrogen on engine performance and emissions in diesel engine. Int J Hydrogen Energy 2020;45:27969–78.
[9] Shadidi B, Najafi G, Yusaf T. A review of hydrogen as a fuel in internal combustion engines. Energies 2021;14:6209.
[10] Wang Y, Gu M, Zhu Y, Cao L, Zhu B, Wu J, et al. A review of the effects of hydrogen, carbon dioxide, and water vapor addition on soot formation in hydrocarbon flames. Int J Hydrogen Energy 2021;46:31400–27.
[11] Liu F, Ai Y, Kong W. Effect of hydrogen and helium addition to fuel on soot formation in an axisymmetric coflow laminar methane/air diffusion flame. Int J Hydrogen Energy 2014;39:3936–46.
[12] Wang Y, Gu M, Chao L, Wu J, Lin Y, Huang X. Different chemical effect of hydrogen addition on soot formation in laminar coflow methane and ethylene diffusion flames. Int J Hydrogen Energy 2021;46:16063–74.
[13] Guo H, Liu F, Smallwood GJ, Gülder ÖL. Numerical study on the influence of hydrogen addition on soot formation in a laminar ethylene–air diffusion flame. Combust Flame 2006;145:324–38.
[14] Ren F, Chu H, Xiang L, Han W, Gu M. Effect of hydrogen addition on the laminar premixed combustion characteristics the main components of natural gas. J Energy Inst 2019;92:1178–90.
[15] Li J, Huang H, Kobayashi N, He Z, Nagai Y. Study on using hydrogen and ammonia as fuels: combustion characteristics and NO_x formation. Int J Energy Res 2014;38:1214–23.
[16] Kalbhor A, van Oijen J. Effects of hydrogen enrichment and water vapour dilution on soot formation in laminar ethylene counterflow flames. Int J Hydrogen Energy 2020;45:23653–73.
[17] Liu B, Liu X, Lu C, Godbole A, Michal G, Teng L. Decompression of hydrogen-natural gas mixtures in high-pressure pipelines: CFD modelling using different equations of state. Int J Hydrogen Energy 2019;44:7428–37.
[18] Clarke MC. Can the hydrogen economy concept be the solution to the future energy crisis? J. Multidiscip. Eng 2022;18:70–84.
[19] Evans MJ, Proud DB, Medwell PR, Pitsch H, Dally BB. Highly radiating hydrogen flames: effect of toluene concentration and phase. Proc Combust Inst 2021;38:1099–106.
[20] Agarwal AK. Biofuels (alcohols and biodiesel) applications as fuels for internal combustion engines. Prog Energy Combust Sci 2007;33:233–71.
[21] Bäckström D, Johansson R, Andersson K, Wiinikka H, Fredriksson C. On the use of alternative fuels in rotary kiln burners—an experimental and modelling study of the effect on the radiative heat transfer conditions. Fuel Process Technol 2015;138:210–20.
[22] Hutny W, Lee G. Improved radiative heat transfer from hydrogen flames. Int J Hydrogen Energy 1991;16:47–53.
[23] Gee AJ, Yin Y, Foo KK, Chinnici A, Smith N, Medwell PR. Toluene addition to turbulent H_2/natural gas flames in bluff-body burners. Int J Hydrogen Energy 2022;47:27733–46.
[24] Gholizadeh M, Hu X, Liu Q. A mini review of the specialties of the bio-oils produced from pyrolysis of 20 different biomasses. Renew Sustain Energy Rev 2019;114:109313.
[25] Czernik S, Bridgwater A. Overview of applications of biomass fast pyrolysis oil. Energy Fuels 2004;18:590–8.
[26] Mohan D, Pittman Jr CU, Steele PH. Pyrolysis of wood/biomass for bio-oil: a critical review. Energy Fuels 2006;20:848–89.
[27] Rana R, Nanda S, Meda V, Dalai A, Kozinski J. A review of lignin chemistry and its biorefining conversion technologies. J. Biochem. Eng. Bioprocess. Technol. 2018;1:2.
[28] Cho S-M, Kim J-H, Kim S-H, Park S-Y, Kim J-C, Choi I-G. A comparative study on the fuel properties of biodiesel from woody essential oil depending on terpene composition. Fuel 2018;218:375–84.
[29] Yin Y, Medwell PR, Gee AJ, Foo KK, Dally BB. Fundamental insights into the effect of blending hydrogen flames with sooting biofuels. Fuel 2023;331:125618.
[30] Zeldvich Y. The oxidation of nitrogen in combustion and explosions. J. Acta Physicochimica 1946;21:577.
[31] Frassoldati A, Faravelli T, Ranzi E. A wide range modeling study of nox formation and nitrogen chemistry in hydrogen combustion. Int J Hydrogen Energy 2006;31:2310–28.
[32] Skottene M, Rian KE. A study of NO_x formation in hydrogen flames. Int J Hydrogen Energy 2007;32:3572–85.
[33] Hashimoto N, Nishida H, Ozawa Y, Iwatsubo T, Inumaru J. Influence of type of burner on NO_x emission characteristics from combustion of palm methyl ester. Int. J. Chem. Mol. Eng. 2009;3:570–4.
[34] McEnally CS, Pfefferle LD. Sooting tendencies of oxygenated hydrocarbons in laboratory-scale flames. Environ Sci Technol 2011;45:2498–503.
[35] Narayanaswamy K, Pitsch H, Pepiot P. A component library framework for deriving kinetic mechanisms for multi-component fuel surrogates: application for jet fuel surrogates, Combust. Flame 2016;165:288–309.
[36] Szymkowicz PG, Benajes J. Development of a diesel surrogate fuel library. Fuel 2018;222:21–34.
[37] Nowakowska M, Herbinet O, Dufour A, Glaude P-A. Detailed kinetic study of anisole pyrolysis and oxidation to understand tar formation during biomass combustion and gasification. Combust Flame 2014;161:1474–88.
[38] Rahman SA, Van TC, Hossain F, Jafari M, Dowell A, Islam M, et al. Fuel properties and emission characteristics of essential oil blends in a compression ignition engine. Fuel 2019;238:440–53.
[39] Lang RJ. Ultrasonic atomization of liquids. J Acoust Soc Am 1962;34:6–8.
[40] Qamar N, Nathan G, Alwahabi Z, King K. The effect of global mixing on soot volume fraction: measurements in simple jet, precessing jet, and bluff body flames. Proc Combust Inst 2005;30:1493–500.
[41] Kent J, Bastin S. Parametric effects on sooting in turbulent acetylene diffusion flames. Combust Flame 1984;56:29–42.
[42] Faravelli T, Frassoldati A, Ranzi E. Kinetic modeling of the interactions between NO and hydrocarbons in the oxidation of hydrocarbons at low temperatures. Combust Flame 2003;132:188–207.

[43] Glaude PA, Pitz WJ, Thomson MJ. Chemical kinetic modeling of dimethyl carbonate in an opposed-flow diffusion flame. Proc Combust Inst 2005;30:1111–8.
[44] Dayma G, Sarathy S, Togbé C, Yeung C, Thomson M, Dagaut P. Experimental and kinetic modeling of methyl octanoate oxidation in an opposed-flow diffusion flame and a jet-stirred reactor. Proc Combust Inst 2011;33:1037–43.
[45] Liu X, Wang H, Yao M. Experimental and modeling investigations on soot formation of ethanol, n-butanol, 2, 5-dimethylfuran, and biodiesel in diesel engines. Energy Fuels 2017;31:12108–19.
[46] Rutkowski L, Khodabakhsh A, Johansson AC, Valiev DM, Lodi L, Qu Z, et al. Measurement of H_2O and OH in a flame by optical frequency comb spectroscopy. CLEO: Sci Innovat 2016:SW4H.8.
[47] Buch R, Hamins A, Konishi K, Mattingly D, Kashiwagi T. Radiative emission fraction of pool fires burning silicone fluids. Combust Flame 1997;108:118–26.
[48] Andersson K, Johansson R, Johnsson F. Thermal radiation in oxy-fuel flames. Int J Greenh Gas Control 2011;5:S58–65.
[49] Park SH, Lee KM, Hwang CH. Effects of hydrogen addition on soot formation and oxidation in laminar premixed C_2H_2/air flames. Int J Hydrogen Energy 2011;36:9304–11.
[50] Dong X, Nathan GJ, Mahmoud S, Ashman PJ, Gu D, Dally BB. Global characteristics of non-premixed jet flames of hydrogen–hydrocarbon blended fuels. Combust Flame 2015;162:1326–35.
[51] Turns SR, Myhr FH. Oxides of nitrogen emissions from turbulent jet flames: Part I—fuel effects and flame radiation. Combust Flame 1991;87:319–35.
[52] Bozzelli JW, Dean AM. O + NNH: A possible new route for NO_x formation in flames. Int J Chem Kinet 1995;27:1097–109.
[53] Wielgosiński G. Pollutant formation in combustion processes. Adv Chem Eng 2012:295–324.
[54] Glarborg P, Miller JA, Ruscic B, Klippenstein SJ. Modeling nitrogen chemistry in combustion. Prog Energy Combust Sci 2018;67:31–68.
[55] Chen C-H, Li Y-H. Role of N_2O and equivalence ratio on NO_x formation of methane/nitrous oxide premixed flames. Combust Flame 2021;223:42–54.
[56] Wagnon SW, Thion S, Nilsson EJ, Mehl M, Serinyel Z, Zhang K, et al. Experimental and modeling studies of a biofuel surrogate compound: laminar burning velocities and jet-stirred reactor measurements of anisole. Combust Flame 2018;189:325–36.
[57] Fu X, Aggarwal SK. Fuel unsaturation effects on NO_x and PAH formation in spray flames. Fuel 2015;160:1–15.
[58] Rahman SA, Mahila T, Ahmad A, Nabi MN, Jafari M, Dowell A, et al. Effect of oxygenated functional groups in essential oils on diesel engine performance, emissions, and combustion characteristics. Energy Fuels 2019;33:9828–34.
[59] Gülder Ö, Snelling D, Sawchuk R. Influence of hydrogen addition to fuel on temperature field and soot formation in diffusion flames. Symp. (Int.) Combust. 1996;26:2351–8.
[60] Mueller ME, Chan QN, Qamar NH, Dally BB, Pitsch H, Alwahabi ZT, et al. Experimental and computational study of soot evolution in a turbulent nonpremixed bluff body ethylene flame. Combust Flame 2013;160:1298–309.